

Visualization of Chladni Patterns at Low-Frequency Resonant and Non-Resonant Flexural Modes of Vibration

Barenten Suciu^{1,*} and Sota Karimine²

ABSTRACT

In this study, Chladni patterns corresponding to resonant and non-resonant vibration modes are visualized on square plates made in steel and aluminum alloys in the low frequency domain of 10–210 Hz. Using a laser sensor, the plate displacement at its central excitation point is measured, and from the obtained frequency response, the resonant and anti-resonant vibration modes are identified. Using the quality-factor method, the damping ratio corresponding to the 1st resonant peak is evaluated. Over a wide range of excitation frequencies, transitions of Chladni figures between resonant patterns via non-resonant patterns could be observed. Such Chladni figures, of the simplest geometrical configuration, can be used to achieve a certain desired movement path of the particles on the vibrating plate by controlling the excitation frequency.

Keywords: Chladni patterns control, Low frequency, Resonant and non-resonant bending vibration modes, Square plate made in steel and aluminum alloys.

Submitted: March 02, 2024

Published: June 09, 2024

 10.24018/ejeng.2024.9.3.3165

¹Department of Intelligent Mechanical Engineering, Faculty of Engineering, Fukuoka Institute of Technology, Japan.

²Graduate School of Engineering, Fukuoka Institute of Technology, Japan.

*Corresponding Author:
e-mail: suciu@fit.ac.jp

1. INTRODUCTION

Chladni patterns are the geometrical figures obtained by sprinkling particles on the surface of a vibrating plate [1], [2]. Using violin bows [1], [3], shakers and speakers [4]–[7], laser beams [8], etc., a stationary flexural vibration mode is to be generated into the horizontally supported plate.

Sprinkled particles, such as sand, salt, and sugar grains [9], silica micro-grains [8], tea powder [7], green soybeans [6], flour, baking soda, and baby powder [10] are usually agglomerating on the plate in the regions of nil or very small amplitude of vibration. Thus, they visualize the nodal lines and produce the so-called standard Chladni patterns, which are dominated by the gravitational effects.

Yet, flexural vibration produces air currents blowing across the plate from nodes to antinodes and then upward. Finer grains, such as dust particles, might be carried by such currents in the regions of large amplitude of vibration, and, as a result, they might visualize the antinodal lines [10].

In fact, the resulting velocity of a particle bouncing on the surface of a vibrating plate depends on the plate velocity, the particle velocity before the impact, and the restitution coefficient of the kinetic energy after impact, which can be perceived as a viscous damping coefficient

[9], [11]. Since the region for particle deposition on the plate depends on the vector of the resultant velocity, the gravitational effect might be diminished.

Similarly, reduction of the gravitational effect on the particle motion can be achieved through buoyancy by submerging the vibrating plate inside a fluidic medium [10], [12]–[15]. Besides, the interaction between a liquid layer and the vibrating plate can be applied to move liquid droplets on it [16], in which case the gravitational effect is diminished by the surface tension contribution. Using these techniques, sophisticated, unconventional Chladni patterns can be easily generated [12]–[16].

The complexity of the Chladni figure depends also on the excitation frequency and the plate shape. Thus, on one hand, frequency augmentation leads to more complex patterns due to the superposition of various degenerate or nearly degenerate eigenmodes [4]–[6]. On the other hand, vibration mode-mixing phenomenon corresponding to a specific geometry of the plate has been reported. Concretely, the vibration mode-mixing is different for triangular plates [5], square plates [4]–[7], rectangular plates [17], hexagonal plates [18], circular plates [7], perforated circular plates [19], violin-like shaped plates [1], [3], [20], etc. Concerning the mode-mixing phenomenon, although

TABLE I: DIMENSIONS OF THE SQUARE PLATES, FREQUENCY INTERVAL EXPLORED, AND RESONANT FREQUENCIES REPORTED BY [4], [7], [25]

Reference	Plate side length L (mm)	Plate thickness h (mm)	Searched frequency range (Hz)	Experimentally found resonant frequencies (Hz)
[4]	240	0.91	1–1000	190, 340, 490, 800, 955
[7]	160	0.61	300–5000	340, 660, 760, 900, 1000, 1450, 1770, 1940, 2540, 3250, 3360, 3430, 3480, 3910, 4178, 4987
[25]	320	1.00	200–3000	363, 592, 701, 776, 1257, 1378, 1553, 1659, 1960, 2451

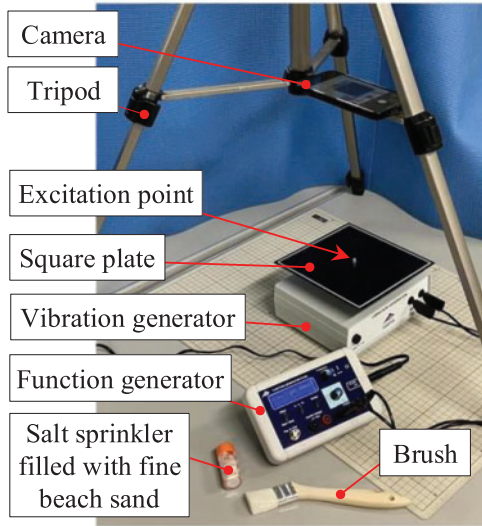


Fig. 1. Photo showing the test rig used to visualize the Chladni patterns.

the plate is excited by a harmonic central source, there are successive backward wave reflections on the boundaries of the plate, directed towards the source, and therefore, superposing on the main central mode. As a result, a dissonant sound that irritates the ear can be perceived during the experiments [9], [18].

Due to their numerous applications in the fields of Civil, Structural, Mechanical, Aerospace, and Seismic Engineering [9], [21]–[28], Chladni patterns appearing at relatively higher resonant frequencies on centrally excited square plates have been extensively studied [4], [7], [25]. Thus, Table I presents the dimensions, i.e., the side length L and thickness h , of various thin square plates made in aluminum, the frequency interval explored in the Chladni tests, and the values of the resonant frequencies, as reported by [4], [7], and [25]. On the other hand, there is quite a wide spectrum of Chladni configurations corresponding to non-resonant frequencies to be used for motion control of objects on vibrating plates in a broad range of applications connected to drug delivery, tissue engineering, microsurgery, micro-robots manipulation, etc. [10], [13]. However, pertinent data necessary for the actual motion control is currently unavailable in the literature.

In this work, an analysis of various flexural vibration modes associated with Chladni patterns occurring on square plates made in aluminum, steel, and stainless steel is performed. In our attempt to visualize the Chladni

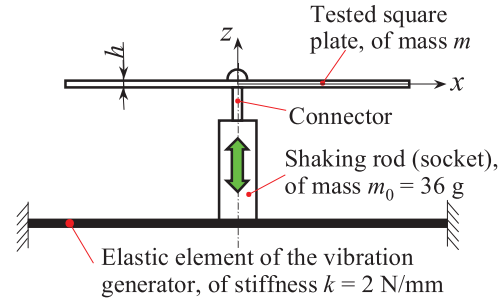


Fig. 2. Vibration model associated to the test rig shown by Fig. 1.

TABLE II: DIMENSIONS AND MATERIAL PROPERTIES OF THE PLATES USED IN THE VISUALIZATION TESTS OF THE CHLADNI PATTERNS

Plate type	P1	P2	P3	P4
Material	Steel S45C	Aluminum alloy, A5052	Stainless steel, SUS304	
Side length, L (mm)	180	180	180	180
Thickness, h (mm)	1.15	1.05	1.05	1.20
Mass, m (g)	262.0	91.7	246.6	300.8
Young modulus of elasticity, E (GPa)	205	70		195
Poisson ratio, μ (–)	0.3	0.33		0.295
Density, ρ (kg/m ³)	7,840	2,660		7,980

patterns, appearing at low frequencies, in the range of 10–210 Hz, fine beach sand is uniformly sprinkled on these square plates, which have the same side length and close thicknesses.

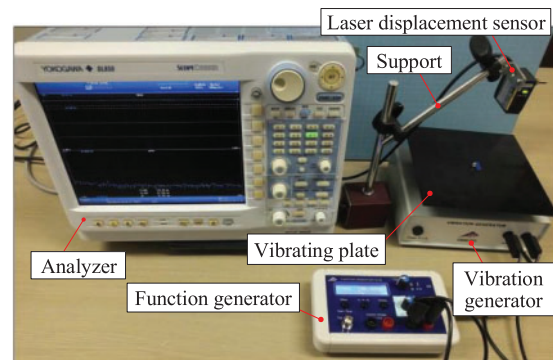


Fig. 3. Photo showing the test rig used to examine the frequency responses (amplitude and vibration level) of the square plates P1–P4.

Several resonant and non-resonant patterns of simple and symmetrical geometry are identified. One experimentally proves that the shape of the Chladni figure changes at augmentation of the excitation frequency. Thus, the circular shape observed at the lowest frequency, is successively shifting into a ring-like shape, then into an elliptical shape, followed by two elliptical-arcs, two parallel segments, two hyperbolic-arcs, and finally is changing into the plate diagonals. These unsophisticated patterns of the simplest geometrical configuration can be used to achieve a certain desired movement path of particles on the vibrating plate by simply adjusting the excitation frequency.

2. TEST RIG AND EXPERIMENTAL PROCEDURE

2.1. Visualization Method of the Chladni Patterns

Fig. 1 shows a photo of the test rig used to visualize the Chladni patterns. By using a salt sprinkler, fine beach sand, with a mean particle diameter of 0.2 mm, is uniformly sprinkled on the plate surface before commencing the

experiments. Flexural vibration of the plate is achieved by employing a 3B-Scientific shaker consisting of a function generator and a vibration generator. At the plate center, a small hole of 3 mm diameter is drilled to horizontally fit the plate above the vertical shaking rod via a banana connector.

Fig. 2 illustrates the vibration model associated with the test rig shown by Fig. 1. The vibration generator consists of an elastic element of stiffness $k = 2 \text{ N/mm}$ and a shaking rod of mass $m_0 = 36 \text{ g}$, which provides the socket necessary to connect the plate. Such a system of two coupled oscillators, consisting of a driving oscillator, i.e., the vibration generator, and a driven oscillator, i.e., the tested elastic plate, is expected to display a complex dynamic behavior with distinctive resonant and anti-resonant frequencies [29]. However, since at very low excitation frequencies, the plate behaves as a rigid element, the frequency of the 1st resonant peak, recorded in our experiments, can be computed as:

$$f_n = \sqrt{k/(m_0 + m)}/(2\pi) \tag{1}$$

Domain of the Chladni patterns		Plate P1 S45C $h = 1.15 \text{ mm}$	Plate P2 A5052 $h = 1.05 \text{ mm}$	Plate P3 SUS304 $h = 1.05 \text{ mm}$	Plate P4 SUS304 $h = 1.20 \text{ mm}$
Circular	Freq. span	100-107 Hz	80-99 Hz	100-129 Hz	140-155 Hz
	Typical figure at a freq. of	107 Hz 	99 Hz 	129 Hz 	155 Hz 
Ring-like	Freq. span	108-144 Hz	102-135 Hz	130-144 Hz	156-174 Hz
	Typical figure at a freq. of	126 Hz 	120 Hz 	141 Hz 	174 Hz 
Elliptical	Freq. span	145-154 Hz	136-137 Hz	145-147 Hz	175-180 Hz
	Typical figure at a freq. of	154 Hz 	137 Hz 	147 Hz 	180 Hz 
Elliptic-arc	Freq. span	155-157 Hz	138-142 Hz	148-150 Hz	181-182 Hz
	Typical figure at a freq. of	157 Hz 	139 Hz 	149 Hz 	182 Hz 
II segments	Freq. span	158-168 Hz	143-149 Hz	151-153 Hz	183-186 Hz
	Typical figure at a freq. of	160 Hz 	145 Hz 	151 Hz 	184 Hz 
Hyperbolic-arc	Freq. span	169-177 Hz	150-172 Hz	154-171 Hz	187-196 Hz
	Typical figure at a freq. of	175 Hz 	165 Hz 	167 Hz 	192 Hz 
X segments	Freq. span	178-181 Hz	173-177 Hz	172-174 Hz	197-207 Hz
	Typical figure at a freq. of	181 Hz 	177 Hz 	174 Hz 	207 Hz 
Recurrent ring	Freq. span	182-210 Hz	178-210 Hz	175-210 Hz	208-210 Hz
	Typical figure at a freq. of	182 Hz 	178 Hz 	175 Hz 	208 Hz 

Fig. 4. Typical Chladni patterns associated with various resonant and non-resonant vibration modes, in the range of 10–210 Hz, for the plates P1–P4.

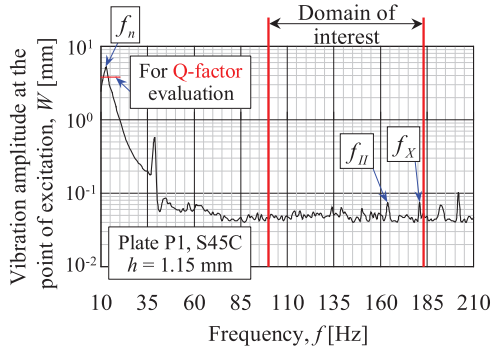


Fig. 5. Variation of the vibration amplitude W , measured at the central point of excitation of the plate P1, versus the frequency f .

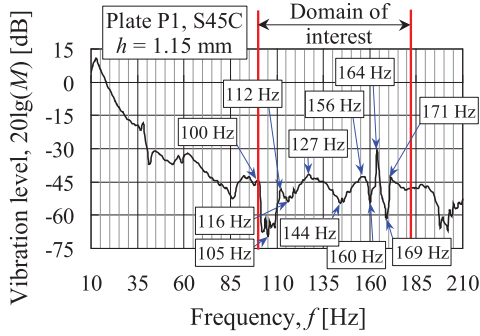


Fig. 6. Variation of the vibration level, determined at the central point of excitation of the plate P1, versus the frequency f .

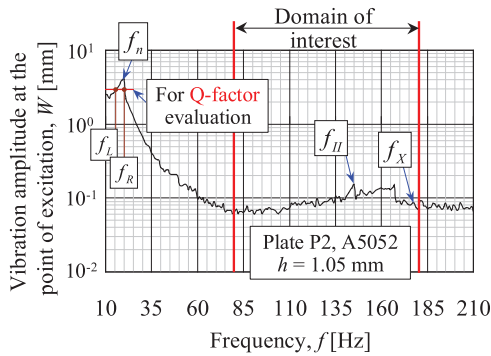


Fig. 7. Variation of the vibration amplitude W , measured at the central point of excitation of the plate P2, versus the frequency f .

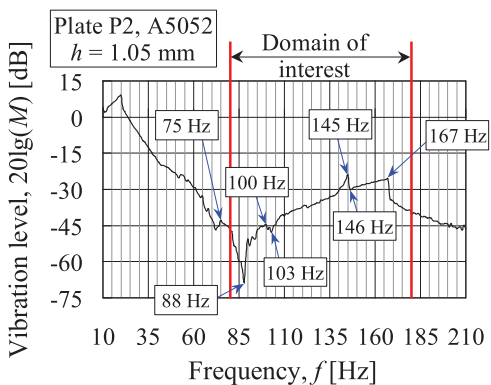


Fig. 8. Variation of the vibration level, measured at the central point of excitation of the plate P2, versus the frequency f .

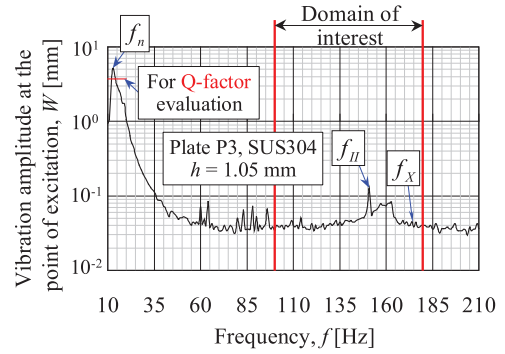


Fig. 9. Variation of the vibration amplitude W , measured at the central point of excitation of the plate P3, versus the frequency f .

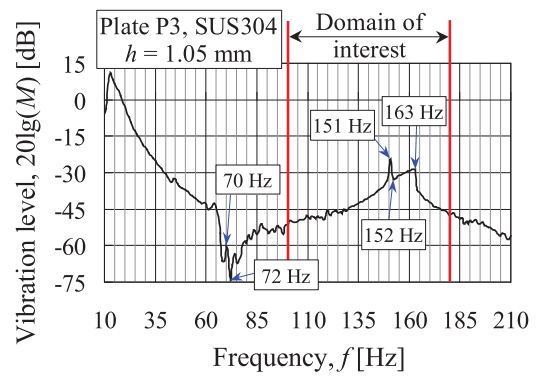


Fig. 10. Variation of the vibration level, measured at the central point of excitation of the plate P3, versus the frequency f .

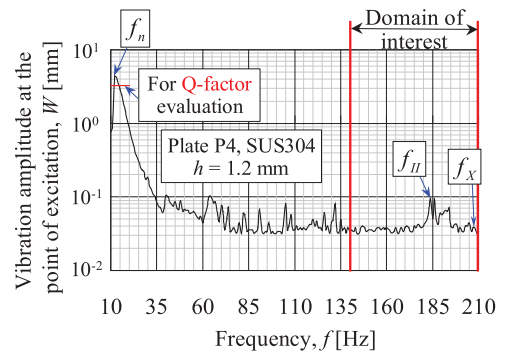


Fig. 11. Variation of the vibration amplitude W , measured at the central point of excitation of the plate P4, versus the frequency f .

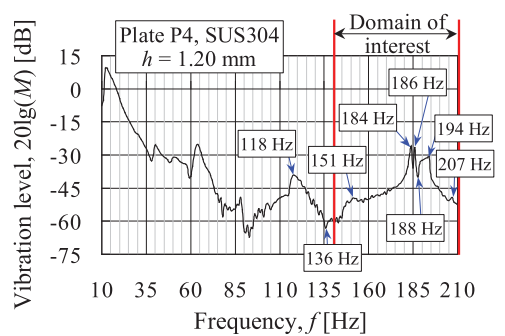


Fig. 12. Variation of the vibration level, measured at the central point of excitation of the plate P4, versus the frequency f .

where m is the mass of the plate.

Table II shows the dimensions and the material properties, i.e., the side length L , thickness h , mass m , Young modulus of elasticity E , Poisson ratio μ , and density ρ of

the square plates used in this work. Tested plates, denoted as P1–P4, are made in carbon steel S45C, stainless steel SUS304, and aluminum alloy A5052. They have the same side length of 180 mm but slightly different thicknesses (see

Table II). In order to achieve good contrast with the grey sand particles, all the tested plates are painted black.

Tests are performed in the low frequency domain, of 10–210 Hz, with a frequency increment of 1 Hz, at the maximal amplitude of excitation, obtained by setting the output signal of the function generator to its maximal value, of 10 V.

A camera, supported by a tripod above the square plate, is used to record the Chladni figure taking form at a certain selected frequency. After each visualization test, conducted at a specific given frequency, the remaining sand is fully removed from the plate surface using a brush.

2.2. Recording Method of the Plate Frequency Response

Fig. 3 shows the test rig used to examine the frequency responses of the plates P1–P4, which are excited in the same way as in the visualization tests of the Chladni patterns.

A laser sensor, Keyence LB-60, is employed to measure the plate displacement at its central excitation point. The output signal of the sensor is amplified and then inputted into an analyzer, Yokogawa DL850, used to perform a Fast Fourier Transform of the recorded time response.

For each plate, two vibration spectra were obtained. One type gives the variation of the vibration amplitude W , and the other type shows the variation of the vibration level $20 \cdot \lg(M)$ [dB] versus the frequency f , at the central point of excitation. Here, M represents the magnification factor [29].

In order to obtain a stationary flexural vibration mode of the tested plate, for each selected frequency in the range of 10–210 Hz, the plate was excited for a time interval of 30 seconds before the signal recording and analysis.

By examining the frequency responses (see Figs. 5–12) of the plates P1–P4, the resonant and anti-resonant bending vibration modes were identified (see Tables III–VI).

3. EXPERIMENTAL RESULTS AND DISCUSSIONS

3.1. Case of Typical Chladni Patterns

Fig. 4 shows the typical Chladni patterns, corresponding to various resonant and non-resonant vibration modes, excited in the range of 10–210 Hz, for all the plates P1–P4.

Figs. 5, 7, 9, and 11 present the variation of the vibration amplitude W versus the frequency f , measured at the central excitation point of plates P1, P2, P3, and P4, respectively.

In order to fully identify the vibration model shown by Fig. 2, damping ratio associated with the 1st resonant peak of the system is clarified, as well. Damping ratio is determined here by using the quality-factor (Q-factor) method [30]. Hence, after finding the maximal amplitude W_{\max} that corresponds to frequency f_n (Figs. 5, 7, 9, and 11), at the intersection of the resonant peak with the red horizontal line that corresponds to an amplitude of $0.707 \cdot W_{\max}$ one finds the left f_L and right f_R frequencies (see Fig. 7), which are used in Tables III–VI to evaluate the Q-factor, and then, the damping ratio.

Additionally, Figs. 6, 8, 10, and 12 show the variation of the vibration level $20 \cdot \lg(M)$ [dB] versus the frequency

TABLE III: RELEVANT FREQUENCY INFORMATION CONCERNING THE CHLADNI PATTERNS AND THE VIBRATION SPECTRA OF THE PLATE P1

Parameter	Values/Range
Lowest frequency for Chladni pattern formation	100 Hz
Domain of interest for Chladni patterns control	100–182 Hz
Frequency of the 1 st resonant peak, f_n (From Fig. 5)	12.9 Hz
Frequency of the 1 st resonant peak, f_n (From (1))	13.0 Hz
Left frequency for Q-factor evaluation, f_L (Fig. 5)	11.3 Hz
Right frequency for Q-factor evaluation, f_R (Fig. 5)	13.8 Hz
Q-factor, $f_n/(f_R - f_L)$; Damping ratio, $0.5(f_R - f_L)/f_n$	5.160; 0.097
Main resonant frequencies in the domain of interest for Chladni patterns control (Fig. 6)	100, 112, 127, 156, 164, 171 Hz
Main anti-resonant frequencies in the domain of interest for Chladni patterns control (Fig. 6)	105, 116, 144, 160, 169 Hz
Domain for the circular Chladni patterns	100–107 Hz
Domain for the ring-like Chladni patterns	108–144 Hz
Domain for the elliptical Chladni patterns	145–154 Hz
Domain for the elliptical-arcs Chladni patterns	155–157 Hz
Domain for the linear Chladni patterns (II type)	158–168 Hz
Frequency of the II type resonant peak, f_{II} (Fig. 5)	164 Hz
Domain for the hyperbolic-arcs Chladni patterns	169–177 Hz
Domain for the diagonal Chladni patterns (X type)	178–181 Hz
Frequency of the X type resonant peak, f_X (Fig. 5)	181 Hz
Domain for the recurrent ring-like Chladni patterns	182–210 Hz
Frequencies for the atypical Chladni patterns	120, 161–167 Hz

TABLE IV: RELEVANT FREQUENCY INFORMATION CONCERNING THE CHLADNI PATTERNS AND THE VIBRATION SPECTRA OF THE PLATE P2

Parameter	Values/Range
Lowest frequency for Chladni pattern formation	80 Hz
Domain of interest for Chladni patterns control	80–178 Hz
Frequency of the 1 st resonant peak, f_n (From Fig. 7)	19.7 Hz
Frequency of the 1 st resonant peak, f_n (From (1))	19.9 Hz
Left frequency for Q-factor evaluation, f_L (Fig. 7)	15.95 Hz
Right frequency for Q-factor evaluation, f_R (Fig. 7)	20.6 Hz
Q-factor, $f_n/(f_R - f_L)$; Damping ratio, $0.5(f_R - f_L)/f_n$	4.237; 0.118
Main resonant frequencies in the domain of interest for Chladni patterns control (Fig. 8)	100, 145, 167 Hz
Main anti-resonant frequencies in the domain of interest for Chladni patterns control (Fig. 8)	88, 103, 146 Hz
Domain for the circular Chladni patterns	80–99 Hz
Domain for the ring-like Chladni patterns	102–135 Hz
Domain for the elliptical Chladni patterns	136–137 Hz
Domain for the elliptical-arcs Chladni patterns	138–142 Hz
Domain for the linear Chladni patterns (II type)	143–149 Hz
Frequency of the II type resonant peak, f_{II} (Fig. 7)	145 Hz
Domain for the hyperbolic-arcs Chladni patterns	150–172 Hz
Domain for the diagonal Chladni patterns (X type)	173–177 Hz
Frequency of the X type resonant peak, f_X (Fig. 7)	177 Hz
Domain for the recurrent ring-like Chladni patterns	178–210 Hz
Frequencies for the atypical Chladni patterns	100, 101 Hz

f , determined at the central point of excitation of the plates P1, P2, P3, and P4, respectively. Such diagrams were obtained by performing a Fast Fourier Transform of the time responses of all plates for each excitation frequency selected to an integer value in the range of 10–210 Hz.

TABLE V: RELEVANT FREQUENCY INFORMATION CONCERNING THE CHLADNI PATTERNS AND THE VIBRATION SPECTRA OF THE PLATE P3

Parameter	Values/Range
Lowest frequency for Chladni pattern formation	100 Hz
Domain of interest for Chladni patterns control	100–175 Hz
Frequency of the 1 st resonant peak, f_n (From Fig. 9)	13.0 Hz
Frequency of the 1 st resonant peak, f_n (From (1))	13.4 Hz
Left frequency for Q-factor evaluation, f_L (Fig. 9)	11.9 Hz
Right frequency for Q-factor evaluation, f_R (Fig. 9)	14.0 Hz
Q-factor, $f_n/(f_R - f_L)$; Damping ratio, $0.5(f_R - f_L)/f_n$	6.190; 0.081
Main resonant frequencies in the domain of interest for Chladni patterns control (Fig. 10)	151, 163 Hz
Main anti-resonant frequencies in the domain of interest for Chladni patterns control (Fig. 10)	152 Hz
Domain for the circular Chladni patterns	100–129 Hz
Domain for the ring-like Chladni patterns	130–144 Hz
Domain for the elliptical Chladni patterns	145–147 Hz
Domain for the elliptical-arcs Chladni patterns	148–150 Hz
Domain for the linear Chladni patterns (II type)	151–153 Hz
Frequency of the II type resonant peak, f_{II} (Fig. 9)	151 Hz
Domain for the hyperbolical-arcs Chladni patterns	154–171 Hz
Domain for the diagonal Chladni patterns (X type)	172–174 Hz
Frequency of the X type resonant peak, f_X (Fig. 9)	174 Hz
Domain for the recurrent ring-like Chladni patterns	175–210 Hz
Frequencies for the atypical Chladni patterns	None

TABLE VI: RELEVANT FREQUENCY INFORMATION CONCERNING THE CHLADNI PATTERNS AND THE VIBRATION SPECTRA OF THE PLATE P4

Parameter	Values/Range
Lowest frequency for Chladni pattern formation	140 Hz
Domain of interest for Chladni patterns control	140–208 Hz
Frequency of the 1 st resonant peak, f_n (From Fig. 11)	12.4 Hz
Frequency of the 1 st resonant peak, f_n (From (1))	12.3 Hz
Left frequency for Q-factor evaluation, f_L (Fig. 11)	11.7 Hz
Right frequency for Q-factor evaluation, f_R (Fig. 11)	14.3 Hz
Q-factor, $f_n/(f_R - f_L)$; Damping ratio, $0.5(f_R - f_L)/f_n$	4.769; 0.105
Main resonant frequencies in the domain of interest for Chladni patterns control (Fig. 12)	151, 184, 186, 194, 207 Hz
Main anti-resonant frequencies in the domain of interest for Chladni patterns control (Fig. 12)	185, 188 Hz
Domain for the circular Chladni patterns	140–155 Hz
Domain for the ring-like Chladni patterns	156–174 Hz
Domain for the elliptical Chladni patterns	175–180 Hz
Domain for the elliptical-arcs Chladni patterns	181–182 Hz
Domain for the linear Chladni patterns (II type)	183–186 Hz
Frequency of the II type resonant peak, f_{II} (Fig. 11)	184 Hz
Domain for the hyperbolical-arcs Chladni patterns	187–196 Hz
Domain for the diagonal Chladni patterns (X type)	197–207 Hz
Frequency of the X type resonant peak, f_X (Fig. 11)	207 Hz
Domain for the recurrent ring-like Chladni patterns	208–210 Hz
Frequencies for the atypical Chladni patterns	None

Tables III–VI present the relevant frequency information concerning the Chladni figures and the vibration spectra of the plates P1, P2, P3, and P4, respectively. The following frequency information was considered as relevant to the present work: the lowest frequency for the Chladni pattern formation; domain of interest to control the shape of Chladni figures of the simplest geometrical

configuration; frequency f_n of the 1st resonant peak as found from tests, and also, by using (1); left and right frequencies (f_L, f_R) used to evaluate the Q-factor, and then, the damping ratio; main resonant and anti-resonant frequencies, inside the domain of interest for pattern control; frequency domains for typical Chladni patterns, i.e., circular, ring-like, elliptical, elliptical-arcs, parallel segments (linear, II-type), hyperbolical-arcs, diagonal segments (linear, X-type), and recurrent ring-like; frequencies of the II- and X-type resonant peaks (f_{II}, f_X); and finally, the frequencies of some atypical Chladni patterns, which were visualized only on the plates P1 and P2.

From Tables III–VI, one notices good agreement between the experimental and theoretical results for the frequency of the 1st resonant peak. As expected, frequency f_n decreases at augmentation of the plate mass m , the highest value of 19.7 Hz being recorded for the lightest plate P2, and the lowest value of 12.4 Hz being obtained for the heaviest plate P4.

Damping ratio varied from the lowest value of 0.081, recorded for plate P3, to the highest value of 0.118, found for plate P2. These values indicate a deviation of about $\pm 19\%$ relative to the average damping ratio, which showed a value of 0.1.

Chladni patterns could be visualized for all the excitation frequencies larger than a certain critical frequency. As shown by the lower value of the frequency span for circular Chladni figures, recorded in Fig. 4, the lowest frequency for pattern formation was found to be 80 Hz for P2, 100 Hz for P1 and P3, and 140 Hz for P4. These values, recorded in the 2nd line of Tables III–VI, are used to define the lower limits for the domains of interest, suggested for Chladni pattern control, as shown by the left-sided red vertical lines in Figs. 5–12.

Fig. 4 provides the experimental evidence that various resonant and non-resonant Chladni patterns of simple and symmetrical geometry, relative to a central Cartesian system of coordinates, taken on the plate surface with the axes parallel to the plate sides, are formed in the range of low frequencies. This result is somewhat unexpected since usually, with very few exceptions, only the resonant Chladni patterns are reported in the literature. Moreover, continuous change of the pattern geometry, gradually leading to shape transitions, was observed at augmentation of the excitation frequency.

Therefore, the visualized Chladni patterns were divided into 8 typical domains. The same sequential transitions from one domain to another, at augmentation of the frequency, have been observed on all four plates, as follows: circular shape at the lowest frequency, changing into a ring-like shape, followed by an elliptical shape, then changing into two elliptical-arcs, followed by two parallel segments, then changing into two hyperbolical-arcs, followed by diagonal segments, and finally changing into a recurrent ring-like shape. For each plate, ranges of variation for the excitation frequency corresponding to all these 8 typical domains are presented in Fig. 4 and also in Tables III–VI.

Resonant flexural modes of the plates P1–P4, indicated in Figs. 5, 7, 9, and 11, as well as in Tables III–VI by the frequency symbols f_{II} and f_X , are of particular interest. They correspond to two types of Chladni patterns consisting of

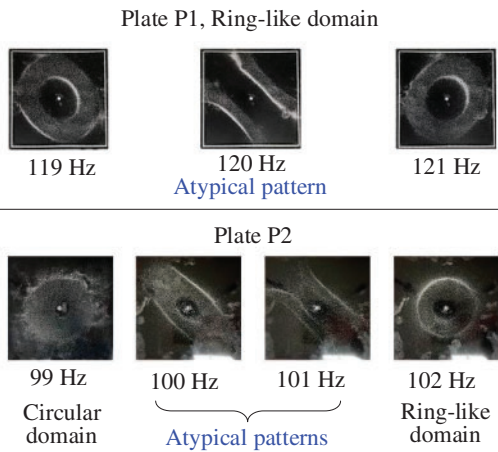


Fig. 13. Atypical Chladni patterns observed inside the ring-like domain of the plate P1, and also, at the transition between the circular and ring-like domains of the plate P2.

straight lines, i.e., parallel and diagonal segments, which were previously reported in the literature [1], [28]. While both theoretical and experimental evidence was provided for the X-type Chladni pattern, only theoretical evidence has been given for the II-type Chladni figure. A reason for this might be the fact that the II-type Chladni pattern is quite difficult to visualize on a plate made of carbon steel. This is indicated in Table III by the atypical Chladni figures occurring around the resonant frequency of 164 Hz, i.e., in the range of 161–167 Hz.

As specified in the last line of Tables III and IV, other atypical Chladni patterns have been observed both on plate P1, at a frequency of 120 Hz, and on plate P2, at a frequency range of 100–101 Hz. Therefore, a detailed discussion concerning this phenomenon is given below.

3.2. Case of Atypical Chladni Patterns

During visualization experiments, some atypical Chladni patterns have been noticed on plates P1 and P2 but not on plates P3 and P4.

For instance, the upper part of Fig. 13 depicts an atypical pattern occurring on plate P1 in the ring-like domain at the excitation frequency of 120 Hz. A similar behavior has been observed on the plate P2 during the transition between the circular and ring-like domains at the excitation frequencies of 100 and 101 Hz. However, since such phenomenon has not been observed during tests carried on plates P3 and P4, it might be regarded as atypical.

Further, Fig. 14 illustrates the atypical Chladni figures visualized around the resonant frequency of $f_{II} = 164$ Hz, on the plate P1. Thus, the parallel segments, observed for frequencies of 159 Hz and 160 Hz, are firstly changing into two vertical elliptical-arcs in the range of 161–163 Hz, which are then changing into two horizontal elliptical-arcs in the range of 163.33–163.6 Hz, through the transitional state consisted of four small vertical elliptical-arcs, noticed at 163.32 Hz. Next, the horizontal elliptical-arcs are changing via similar transitional states, appearing in the range of 163.65–163.66 Hz, into the resonant pattern ($f_{II} = 164$ Hz) consisting of four small circles. Then, these circles are gradually degenerating into four small ellipses (see the range of 164.3–165.3 Hz). Next, this configuration evolves into the

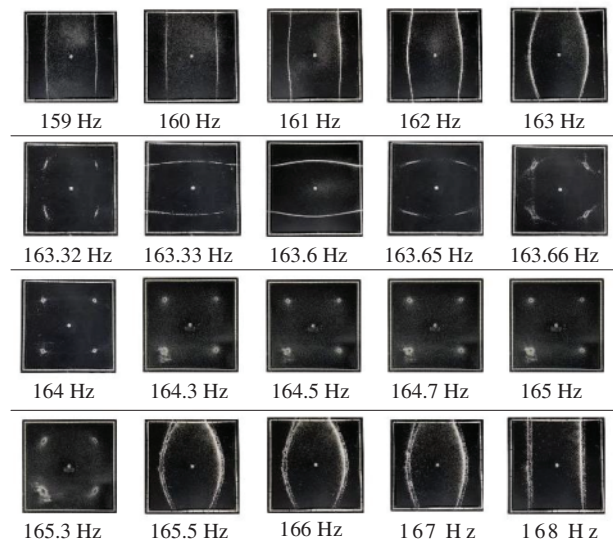


Fig. 14. Atypical Chladni patterns observed around the resonant frequency of $f_{II} = 164$ Hz, on the plate P1.

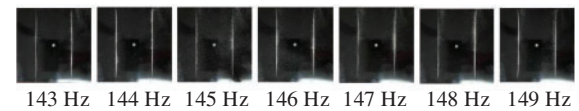


Fig. 15. Typical Chladni patterns observed around the resonant frequency of $f_{II} = 145$ Hz, on the plate P2.

recurrent patterns composed of two vertical elliptical-arcs in the range of 165.5–167 Hz and, finally, into two parallel segments at a frequency of 168 Hz.

Note that such complex transitions of patterns, occurring at quite small frequency increments, have not been observed during tests carried out on plates P2, P3, and P4. Therefore, this phenomenon might be regarded as atypical. For instance, Fig. 15 provides the experimental evidence that there is no change of the Chladni figures, visualized on the plate P2, in the range of 143–149 Hz, i.e., around the resonant frequency of $f_{II} = 145$ Hz (see also Figs. 7, 8 and Table IV).

4. CONCLUSION

In this work, Chladni patterns associated to resonant and non-resonant flexural vibration modes were visualized on square plates made in steel and aluminum alloys in the low frequency domain of 10–210 Hz.

Using a laser sensor, the plate displacement at its central excitation point was measured, and two types of vibration spectra, one showing the variation of the vibration amplitude and the other presenting the variation of the vibration level versus the excitation frequency, were obtained. Based on such diagrams, the resonant and anti-resonant bending vibration modes were clearly identified.

A vibration model associated with the test rig, used to visualize the Chladni patterns, was proposed. Stiffness and damping ratio, corresponding to such a model of the dynamic system, were identified by using the frequency of the 1st resonant peak and the quality-factor method, respectively.

For excitation frequencies exceeding a certain critical value, not only resonant but also non-resonant Chladni patterns of simple and symmetrical geometry were noticed.

Continuous change of the pattern geometry, gradually leading to shape transitions, was observed at augmentation of the excitation frequency. Therefore, these Chladni figures were divided into 8 typical domains, according to their specific shape, as follows: circular, ring-like, elliptical, two elliptical-arcs, two parallel segments, two hyperbolic-arcs, diagonal segments, and recurrent ring-like.

Control of the micro-particle motion on the vibrating plate by adjusting the excitation frequency was suggested as a possible actual application for these Chladni patterns of simple geometry and fair sensitivity at the frequency change.

Atypical Chladni figures were observed on the plate made of carbon steel, especially around the resonant frequency related to the pattern consisting of two parallel segments. One suggested that this might be the reason for the lack of experimental evidence in the surveyed literature for this resonant flexural mode of the lowest frequency.

CONFLICT OF INTEREST

The authors declare that they do not have any conflict of interest.

REFERENCES

- [1] Chladni EFF. *Discoveries about the Theory of Sound*. Leipzig: Breitkopf und Härtel; 1787.
- [2] Faraday M. On a peculiar class of acoustical figures. *R Soc London*. 1831;121:299–340.
- [3] Molin NE, Lindgren LE, Jansson EV. Parameters of violin plates and their influence on the plate modes. *J Acoust Soc Am*. 1988;83:281–91.
- [4] D'Alessio SJD. Forced free vibrations of a square plate. *SN Appl Sci*. 2021;3(60):6 1–14.
- [5] Tuan PH, Tung JC, Liang HC, Chiang PY, Huang KF, Chen YF. Resolving the formation of modern Chladni figures. *EPL A. Lett J Explor Front Phys*. 2015;111(6):64004.1–6.
- [6] Tuan PH, Wen CP, Chiang PY, Yu YT, Liang HC, Huang KF, et al. Exploring the resonant vibration of thin plates: reconstruction of Chladni patterns and determination of resonant wave numbers. *J Acoust Soc Am*. 2015;137(4):2113–23.
- [7] Kumar A, Chary SS, Wani KP. Modal analysis of Chladni plate using Cymatics. *SAE Tech*. 2020;28:0320.1–7.
- [8] Shu YH, Tseng YC, Lai YH, Yu YT, Huang KF, Chen YF. Exploring the origin of maximum entropy states relevant to resonant modes in modern Chladni plates. *Entropy*. 2022;24(2):1–15.
- [9] Ikpe AE, Ndon AE, Etuk EM. Response variation of Chladni patterns on vibrating elastic plate under electro-mechanical oscillation. *Niger J Tech*. 2019;38(3):540–8.
- [10] Zhou Q, Sariola V, Latifi K, Liimatainen V. Controlling the motion of multiple objects on a Chladni plate. *Nat Commun*. 2016;7:12764 1–10.
- [11] Shridhar M. Manipulating standard and inverse Chladni patterns by modulating adhesive, frictional, and damping forces. *Int J Sci Eng Res*. 2011;3(5):782–9.
- [12] Vuillermet G, Gires PY, Casset F, Poulain C. Chladni patterns in a liquid at microscale. *Phys Rev Lett*. 2016;116(18):184501.1–5.
- [13] Usadi LN, Yee S, Elbidweithy H, Firebaugh S. Manipulation of microrobots using Chladni plates and multimode membrane resonators. *Eng Proc*. 2021;4(39):09593.1.
- [14] Latifi K, Wijaya H, Zhou Q. Motion of heavy particles on a submerged Chladni plate. *Phys Rev Lett*. 2019;122(18):184301.1–5.
- [15] Escaler X, De La Torre O. Axisymmetric vibrations of a circular Chladni plate in air and fully submerged in water. *J Fluids Struct*. 2018;82:432–45.
- [16] Scortesse J, Manceau JF, Bastien F. Interaction between a liquid layer and vibrating plates: application to the displacement of liquid droplets. *J Sound Vibr*. 2002;254(5):927–38.
- [17] Mama BO, Onah HN, Ike CC, Osadebe N. Solution of free harmonic vibration equation of simply supported Kirchhoff plate by Galerkin-Vlasov method. *Niger J Tech*. 2017;36(2):361–5.
- [18] Cuenca J. Wave models for the flexural vibrations of thin plates—model of the vibrations of polygonal plates by the image source method and vibration damping using the acoustic black hole effect. Ph.D. Thesis, Du Maine University, France; 2009.
- [19] Kaczmarek A, Javorek L, Orłowski K. Mode vibrations of plates—experimental analysis. *Ann Warsaw Univ Life Sci*. 2014;88:97–101.
- [20] Stylianides A, Milanovic I, Celmer R. An investigation of violin sound quality through resonant modes. *Proc of the COMSOL Conf*, pp. 2113–23, Boston, USA, 2019.
- [21] Chakram S, Patil YS, Chang L, Vengalattore M. Dissipation in ultrahigh quality factor SiN membrane resonators. *Phys Rev Lett*. 2014;112:127201.1–8.
- [22] Dorrestijn M, Bietsch A, Aelkalin T, Raman A, Hegner M, Meyer E, et al. Chladni figures revisited based on nanomechanics. *Phys Rev Lett*. 2007;98:026102.1–4.
- [23] Flores J. Nodal patterns in the seismic response of sedimentary valleys. *Eur Phys J Spec Top*. 2007;145:63–75.
- [24] Szilard R. *Theories and Applications of Plate Analysis*. New York: John Wiley & Sons; 2004.
- [25] Tseng YC, Hsu YH, Lai YH, Yu YT, Liang HC, Huang KF, et al. Exploiting modern Chladni plates to analogously manifest the point interaction. *Appl Sci*. 2021;11(21):1–12.
- [26] Timoshenko S, Woinowsky-Krieger S. *Theory of Plates and Shells*. 2nd ed. New York: Mc-Graw Hill; 1987.
- [27] Tuan PH, Lai YH, Wen CP, Huang KF, Chen YF. Point-driven modern Chladni figures with symmetry breaking. *Sci Rep*. 2018;8(1):1–13.
- [28] Waller MD. Vibration of free square plates: part I. Normal vibrating modes. *Proc Phys Soc*. 1939;51(5):831–44.
- [29] Ewins DJ. *Modal Testing: Theory and Practice*. New York: John Wiley & Sons; 1984.
- [30] Siebert W. *Circuits, Signals, and Systems*. Massachusetts: MIT Press; 1985.